ETH
Eidgenössische Technische Hochschule Zürich
Swiss Federal Institute of Technology Zurich

Empa
Materials Science and Technology

Timon Schär

Numerical Analysis of Residual Stress and Distortion in Laser Powder Bed Fusion Process: A Sensitivity Analysis to the Choice of Constitutive Model

Bachelor's thesis

Institute of Mechanical Systems
Swiss Federal Institute of Technology (ETH) Zurich

Advisors

Prof. Dr. E. Mazza, Dr. E. Hosseini, P. Markovic

Institute of Mechanical Systems, ETH Zürich
Experimental Continuum Mechanics, Empa

May 25, 2022

Abstract

In this work, the sensitivity of residual stress and distortion development to the choice of constitutive model using thermomechanical simulations of laser powder bed fusion additive manufacturing was investigated. A multi-layer single track finite element model was set up and the simulated residual stresses and plastic strains were compared for various sets of material models of Hastelloy X, which were calibrated using tensile test data. In particular, the qualitative influence of the Bauschinger effect was examined by comparing isotropic with kinematic hardening models, which revealed large deviation in residual stress for multi layer simulations. Additionally, the influence of creep on simulation results was investigated using the Norton creep law. Although comparably high creep strain rates where recorded in the vicinity of the localised heat input, the total accumulated creep strain was found to be negligible as a result of the rapid cool-down. Finally, the influence of the materials annealing behaviour at elevated temperatures was studied by introducing an anneal temperature with various values. This had an immense effect on the equivalent plastic strain, showing a nearly linear dependence between anneal temperature and equivalent plastic strain.

Acknowledgment

First, I want to thank Professor Edoardo Mazza for providing the opportunity for this exceptional learning experience in his research group. I am also very thankful towards Dr. Ehsan Hosseini for always having an open ear for my questions and for reminding me not to be satisfied too early. I also especially want to thank Patrik Markovic for his warm and motivating support, giving many valuable tips and tricks along the way and helping me to see the bigger picture.
My gratitude also goes towards the other staff of the High Temperature Intergrity Group for their kind welcome and generous support.
Thank you.
Timon Schär

Contents

1. Introduction

Metal Additive Manufacturing (MAM), colloquially known as 3D-printing, is a production process that has been heavily researched in the past two decades and finds more and more its way into industrial applications [1, 2]. During fabrication, a part is built up layer by layer in an additive manner using structural data from a 3D model. Laser Powder Bed Fusion (LPBF), also referred to as Selective Laser Melting (SLM), is a process in the field of MAM. In order to build up a part, a bed of metal powder is melted selectively by a laser. A roller then adds the next layer of powder to the bed. This process is repeated until the whole part is created, as depicted in figure 1.1.
Compared to conventional manufacturing, MAM has many advantages. It allows the manufacturing of parts with very little constraints on form such as round holes or straight edges, which enables engineers to utilize highly optimized shapes and structures and often drastically reduce the part count. No custom tooling is necessary, e.g. molds, which allows inexpensive customization of individual parts. This is extremely beneficial for medical applications, such as implants which can be personalized for each patient [4], efficient repairing of complex machines [5], or rapid prototyping in general. In contrast to subtractive processes, e.g. milling, the resulting amount of waste material is very low. Beside its great advantages, MAM has significant downsides, which currently inhibit large scale commercial application. To begin with, the costs are very high without any significant scale effect for large quantities [6]. MAM is therefore only cost-effective for specialized, small batch applications. What's more, manufacturing time per part is very high, which again limits the producible quantities. This can be counteracted by reducing the part count, which in turn reduces assembly time [7]. Finally, the LPBF process leads

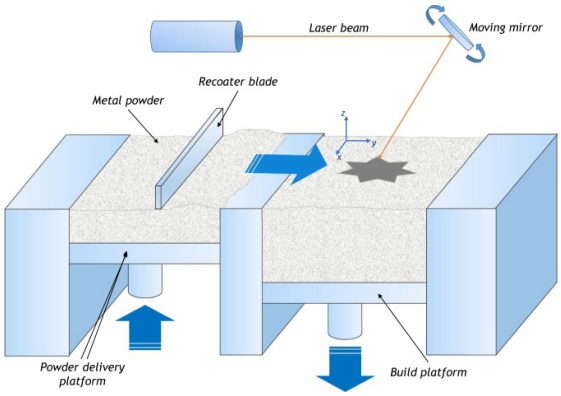

Figure 1.1: LPBF schematic [3]

to large residual stresses in the material, which cause deformation and reduced strength, or might lead to delamination of the part and crack formation during printing [8]. This is the most pertinent challenge for industrial applications, as mechanical integrity and precision are crucial for typical MAM applications.
Unparalleled by conventional processes, large temperature gradients evolve upon localised heat input inherent to the LPBF process and are responsible for the high residual stresses. While it is possible to reduce residual stresses significantly by in-situ control methods or post-processing heat treatments [9], the resulting change in shape and the possibility of cracks or fractures can make the application of LPBF extremely difficult. Often, an acceptable build quality is only achieved after multiple, expensive trial and error iterations. A deeper understanding of the residual stress development associated with MAM process might be achieved through numerical simulations, which would in turn enable a more systematic optimisation of process conditions required to reach the goal of 'fist-time-right' high-quality production.
Simulations of LPBF processes are usually done using the finite element method (FEM), as it can handle substantial nonlinearities exceptionally well. FEM is a method of dividing a large continuous model into a mesh of small standardised elements. Since the behaviour of a single element is known, it is possible to estimate the behaviour of the full model. Sophisticated commercial computer programs are available which allow straightforward implementation and execution of such simulations. Some even offer a dedicated AM modelling tool.
In order for the simulation to give meaningful results, a comprehensive constitutive material model must be given. A great number of models exist, each with a different level of accuracy and complexity. It is unclear what the influence of the choice of model is on the simulation results in MAM. What's more, research on MAM residual stress simulation is often conducted without any justification why a particular model has been chosen, in turn neglecting the significance of this decision. It is suspected that simulation errors can be greatly reduced by using an adequate material model. P. Promoppatum and A. Rollett [10] studied the sensitivity of constitutive models on thermomechanical responses in LBPF simulations by comparing multiple models fitted to the same data, and found significant differences in predicted stresses. However, the models they investigated where all based on isotropic hardening, thus neglecting cyclic Bauschinger effects upon reversed loading. Yet it has been shown that the LBPF process is of cyclic nature, as each layer experiences stresses induced by each consecutively printed layer [11]. The present work tries to determine the importance of cyclic effects by comparing two fundamental constitutive models, namely nonlinear isotropic and kinematic hardening. Second, creep effects are examined as they too are not considered in current research. It is unclear whether the high stresses and temperatures during the LPBF process lead to significant creep strain because of the raped cool-down. For a different MAM process, Springer et al. observed considerably smaller simulation errors when including creep [12], and it needs to be checked if these findings can be applied to LPBF. As a third feature of constitutive models, the influence of the material's annealing behaviour was investigated. Work hardened metals undergo annealing at high temperatures through reduction of dislocation density and recristallization. In the model, a temperature was defined at

which the hardening memory and accumulated plastic strain is reset. This is a common practice for weld simulations, but seldom mentioned in studies on LPBF simulation.

2. Experimental Data

The sensitivity of LPBF simulations to these constitutive model features are studied by setting up an adequate Model in the commercial FEM software Abaqus using its AM Modeler, and running simulations with various parameter configurations. It was thus possible to conclude the relative importance of each studied feature of constitutive models. The constitutive model was calibrated using the first half-cylce data form a cyclic tension-compression test with strains reaching a magnitude of 0.75 % at a strain rate of 0.005 s^{-1}, with a hold time of 900 s at maximum strain. The test was conducted using samples of Hastelloy X produced by LPBF. As the LPBF process inherently involves a broad range of temperatures and the material properies depend widely on temperature, test data was obtained at seven temperatures, ranging from room temperature up to 1000°C (Table 2.1).

22	200	400	600	800	900	1000

Table 2.1: Measured Temperatures [°C]

3. Constitutive Model Formulation and Calibration

3.1. Isotropic and Kinematic Hardening Model

Simple elasto-plastic models with nonlinear kinematic and isotropic hardening rules have been chosen as constitutive models to determine the significance of cyclic and reverse-loading effects in thermomechanical simulations of LPBF. A metal deforms elastically when it is subjected to mechanical stresses, as described by Hooke's Law,

$$\epsilon = \sigma / E, \tag{3.1}$$

where ϵ is elastic strain, σ is stress and E is young's modulus. For stresses beyond the elastic limit, this proportional law no longer holds as the metal yields and plasticity occurs. Through plastic deformation, the material hardens. As a result, the yield strength will be higher after previous loading and unloading. On the other hand, when the metal is first hardened by tensile stresses and then compressed, the compressive yield strength will be lower. This behavior is generally referred to as the "Bauschinger Effect". The yield strength can be generalized into a three dimensional yield surface. The difference of isotropic and kinematic constitutive models lies in the reaction of the yield surface to plastic straining, as depicted in Fig. 3.1. For an isotropic model, the yield surface enlarges, leading to equal hardening in each direction. In contrast, the more complex kinematic model reacts by shifting the yield surface. This leads to hardening in the strain direction and softening in the opposite direction, thus representing the Bauschinger effect. Often, the two models are combined for a better accuracy.
Abaqus provides multiple implementations of these models, with either linear, multilinear or nonlinear hardening [14]. For this study, nonlinear hardening is chosen for its smooth

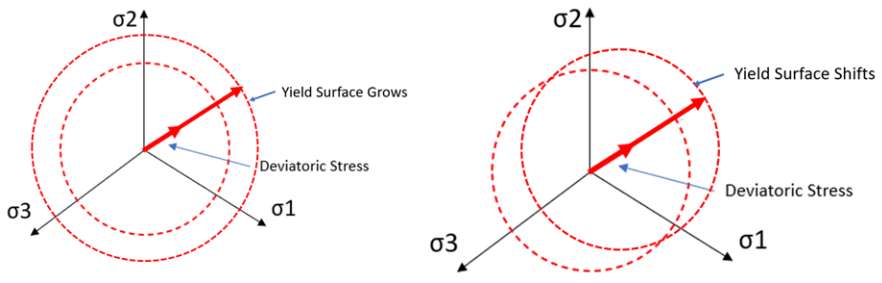

Figure 3.1: Transformation of the yield surface and the elastic domain in the deviatoric stress plane by purely isotropic (left) and kinematic (right) ardening [13].

behaviour and because it enables introducing the anneal temperature, which is also fundamental for the study. The provided simple exponential law was used for the yield surface size development. The nonlinear isotropic/kinematic hardening model is set up as a combined model, but it can be used as a purely isotropic model by setting the kinematic hardening to zero, and vice versa. For isotropic hardening, the size of the yield surface is given as

$$\sigma^0 = \sigma_y + Q_\infty(1 - e^{-b\epsilon_{pl}}), \tag{3.2}$$

where σ_y is the yield surface size at zero plastic strain, ϵ_{pl} is the equivalent plastic strain and Q_∞ and b are material parameters. For kinematic hardening, the rate of change of the backstress α can be given in a simplified form as

$$\dot{\alpha} = C\frac{1}{\sigma^0}(\sigma - \alpha)\dot{\epsilon}_{pl} - \gamma\alpha\dot{\epsilon}_{pl}, \tag{3.3}$$

where C and γ are material parameters [14].

3.2. Hardening Model Calibration

For the purpose of calibration, the kinematic model given in equation (3.3) can be integrated over the first half cycle, which results in a curve similar to the isotropic model:

$$\sigma^0 = \sigma_y + \frac{C}{\gamma}(1 - e^{-\gamma\epsilon_{pl}}). \tag{3.4}$$

It is possible to calibrate only the isotropic model and deduce the kinematic model parameters later on. By a simple parameter transformation, identical behavior for both models is ensured over the first half cycle, such that the only difference in the models is in the cyclic behaviour:

$$\gamma = b, C = Q_\infty b \tag{3.5}$$

Because of the wide range of occurring temperatures and large temperature gradients during the LPBF process, it is crucial that the temperature dependence of the material parameters is treated well. Experimental data was available at a range of seven temperatures reaching from room temperature to $1000°C$. Using Matlab's "surrogateopt"-algorithm, the RMS error between experimental and model behavior was minimised at each measured temperature. To ensure a smooth parameter development, all parameters were constrained to an exponential temperature dependence as in equation (3.6), resulting in 18 degrees of freedom in total.

$$k(T) = u(1 - ve^{-T/w}) + x(1 - ye^{-T/z}) \tag{3.6}$$

Here, the variables u,v,w and x,y,z are the parameters of the implemented double exponential law. Using this procedure, a good fit was possible for all available temperatures, except for high temperatures above $900°C$, where the exponential trend could no longer be sustained. For the data point at $1000°C$, the parameters σ_y and b where calculated without any constraints. The parameters obtained this way are shown in Fig. 3.2.

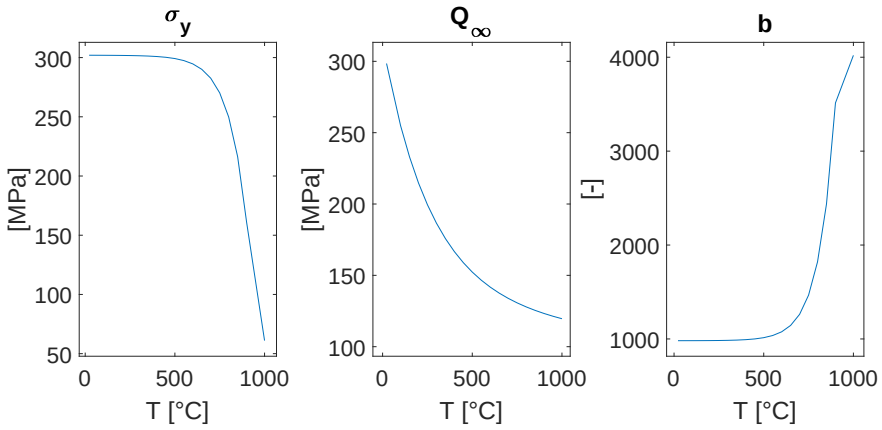

Figure 3.2: Optimized isotropic hardening law parameters with (exponential) temperature dependence.

For simplicity, the model was calibrated only to the first half cycle of experimental data. As can be seen in Fig. 3.3, the resulting model is able to handle cyclic loading reasonably well.

3.3. Creep Model

Creep is visco-plastic straining caused by diffusive, time dependent processes, which already occur at stresses below yield strength. The Norton creep law is a mathematical model widely used to describe this material property as it is remarkably simple. It is not suitable to model creep under cyclic loading, so in this study, simulations using creep were done only for a single layer. By this law, the creep strain rate can be formulated as

$$\dot{\epsilon}_{cr} = A\sigma^n, \tag{3.7}$$

where A and n are temperature dependent material parameters. Because the parameter A can get extremely small for low temperatures, Abaqus provides a mathematical reformulation called "power law" to avoid numerical issues [14], which was used in this work. It is crucial to choose the strain hardening form, as the stresses vary widely over time for LPBF.

3.4. Creep Model Calibration

Data from the same experiment used in section 3.2 to calibrate the hardening model was also used to determine the Norton creep parameters. For that purpose, the probes were held at a constant strain of 0.75% for 900 seconds after the initial tensile test and the relaxation of stresses was measured. By using equation (3.1), the Norton creep law

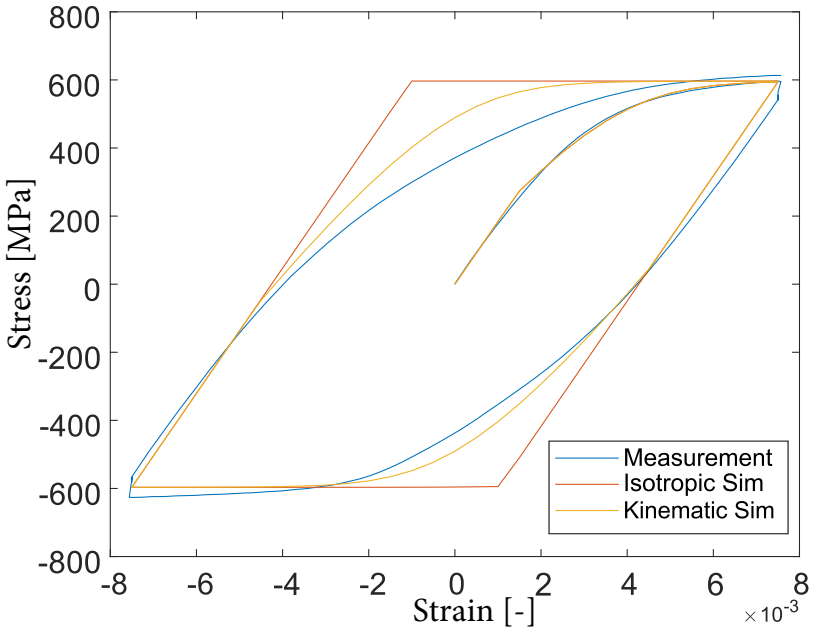

Figure 3.3: Measured and simulated tensile test at $23°C$. In the experimental data, the stress relaxation during the hold time is visible, which is not considered in these simulations.

was integrated into the relaxation form (Equation 3.8) which could then be fitted to the experimental data, as seen in Fig. 3.4.

$$\sigma(t) = ((n-1)AEt + \sigma_i^{1-n})^{\frac{1}{1-n}} \tag{3.8}$$

Here, σ_i is the initial stress at $t = 0$. Similar to the optimization procedure applied to the elasto-plastic model with hardening, the RMS error between the predicted and measured stress relaxation was minimized using the "surrogateopt" algorithm of Matlab for each measured temperature. The parameters were again constrained to an exponential temperature dependence, whereby the best option found was to apply this constraint to the decimal logarithm of A. For low temperatures below $600°C$, it was observed that the best fit would be possible for values of the parameter n greater than 100. For such high values of the stress exponential, the Norton creep law shows highly unstable behavior as the creep strain rate becomes excessively dependent on stress levels. To ensure stability, the parameter n was held at a constant value for temperatures below $600°C$. The final creep parameters are depicted in the plot on the left in Fig. 3.4.

3.5. Annealing Effect

At high temperatures close to the melting point, accumulated work hardening is annealed through recovery of dislocations and recristallization. This needs to be treated

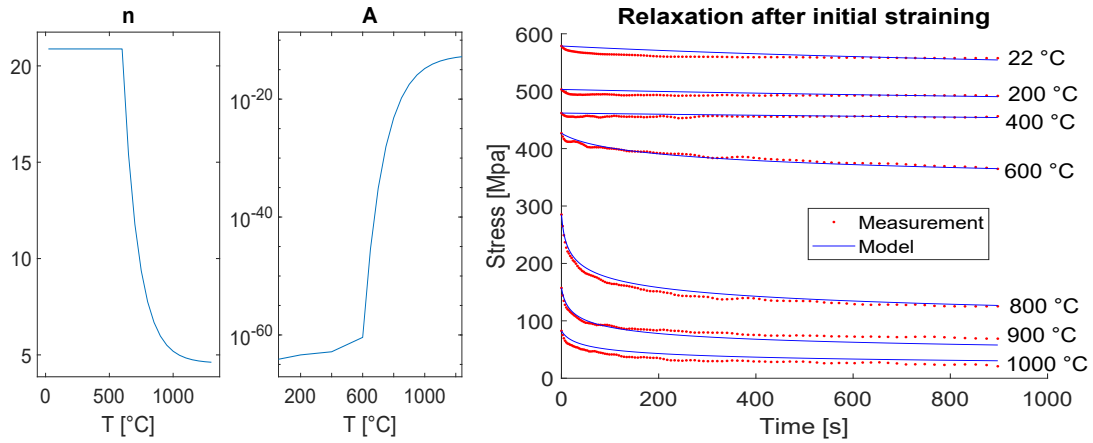

Figure 3.4: Optimized Norton creep parameters with (exponential) temperature dependence (left), Experimental and model relaxation curves (right).

for FEM simulations, as it will lead to an overestimation of plastic straining when the material is allowed to harden beyond such temperatures. In Abaqus, it is possible to implement a very simple model of annealing effects by setting an anneal temperature. When the temperature at an integration point goes over this threshold, Abaqus will reset the accumulated plastic strain (PEEQ) to zero and will only restart to accumulate plastic strains once the temperature falls again below this point. Additionally, all hardening history is reset. The hardening parameters need to be given such that there is no hardening above the anneal temperature. As this model is such a strong simplification, it is unclear, what physical property of a metal resembles to this parameter. Because this study focuses on the significance of each simulation parameter, five different anneal temperatures have been chosen over a broad temperature range. These five values are both the solidus and liqiudus temperature at $1260°C$ and $1355°C$ respectively [15], further a recommended temperature for annealing heat treatments at $1175°C$ [16] as well as $1050°C$, where partial elimination of dislocations was observed by Cheng et al. [17]. Note that the latter two temperatures are given for processes over the duration of one hour, so their application to LPBF is only for comparative purposes. Additionally, a simulation was conducted without considering annealing at all.

4. Simulation Setup

FEM simulations were conducted using the AM modeler plugin of Abaqus. By this plugin, the thermal and mechanical analysis are performed sequentially assuming only one-way coupling, which means that the heat generated by deformation is neglected. The model consists of a base plate and five layers of single-track printed material. For some simulations, only one layer is simulated. The tracks have a total length of 1.5 mm and a print length of 1.3 mm, a width of 0.2 mm and the layer thickness is 0.03 mm. The mesh was chosen such that the mesh size at the track is equal to the layer thickness, with increasing size towards the edges of the base plate (Fig. 4.1). For the thermal simulation, linear elements have been chosen, and for the mechanical simulation, quadratic elements have been chosen, each with full integration.
All parameters for the AM modeler plugin and some material properties were provided by P. Gh. Ghanbari, which can be found in the appendix (Table A.1). Subsequent activation of each layer which models a roller applying a layer of powder, followed by the laser modelled by a Goldak heat source is provided by the AM plugin. The laser moves with a speed of 1000 mm/s, taking 1.3 ms per layer. Each activation is set to a duration of 0.9987 s, such that the laser pulse followed by the roller take up one second, such that the printing of five layers adds up to five seconds of simulated time. After printing, the model is allowed to cool down for five seconds, after which the whole model is again at

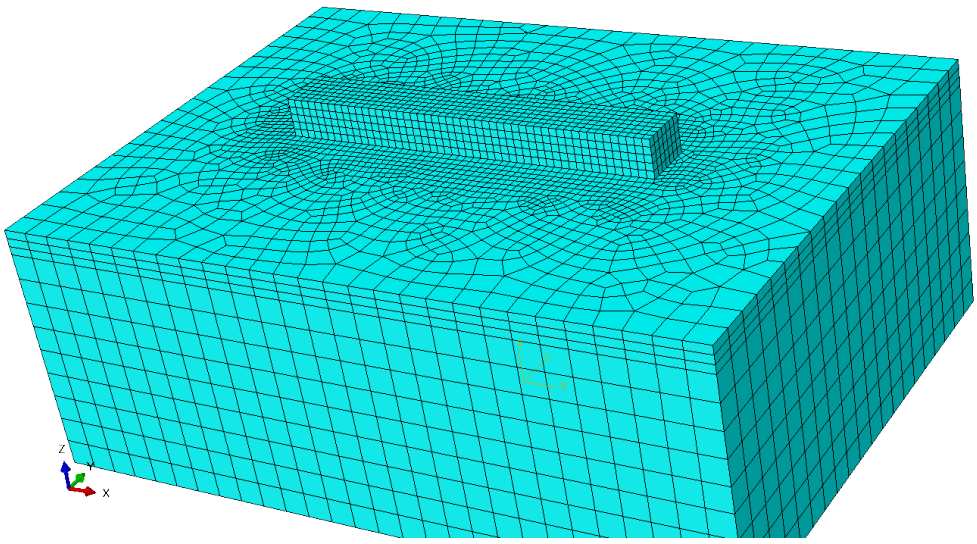

Figure 4.1: Five layer single track mesh

room temperature.
In all simulations, parabolic extrapolation was enabled, as well as nonlinear geometries for the mechanical analysis. For simulations using the kinematic hardening model, it was necessary to use automatic stabilization to reach a converged simulation. To stabilize, Abaqus includes artificial damping. Even though stabilization was not needed for isotropic simulations, it was still included in the simulations to ensure comparability between models with kinematic or isotropic hardening rules. Furthermore, it was made sure that the damping energy was comfortably below one percent of total strain energy.

5. Results and Discussion

5.1. Data Preparation

Towards the edges of the track, the stress and strain distribution is largely dominated by boundary effects. To reduce the influence of the geometry, all simulation data presented below are taken from the central element on the lowest printed layer, in particular from its integration point (IP) at the center of the cube element, . The black arrow in Fig. 5.1 points to this IP. An IP was chosen instead of nodes as the values at the integration points are actually calculated, while the nodal values are extrapolated from these values. Data from this IP can be plotted showing the development of a variable over time. In the case of Mises stress, a large part of the observed development can be attributed directly to the temperature field and the corresponding saturated stress of the hardening model at each temperature. The hardening models are observed to saturate quickly after about 1%. As the strain levels during LPBF reach up to 10%, it can be seen in Fig. 5.2 that the constitutive model saturates quickly during the laser pulse and follows the temperature induced saturation curve during cool-down.

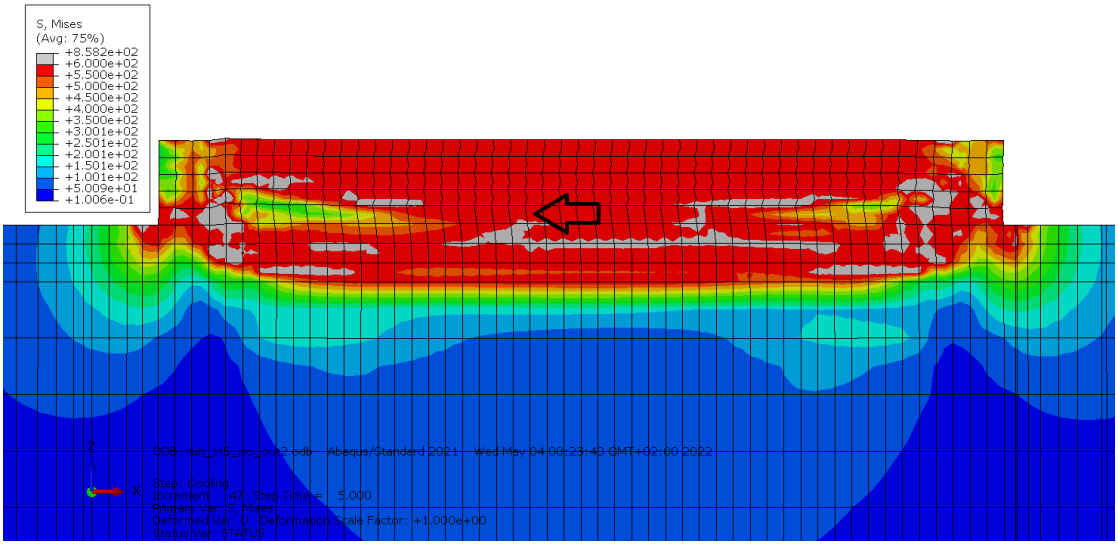

Figure 5.1: Cut through model: residual Mises stress distribution. The arrow points to the integration point where the data was acquired.

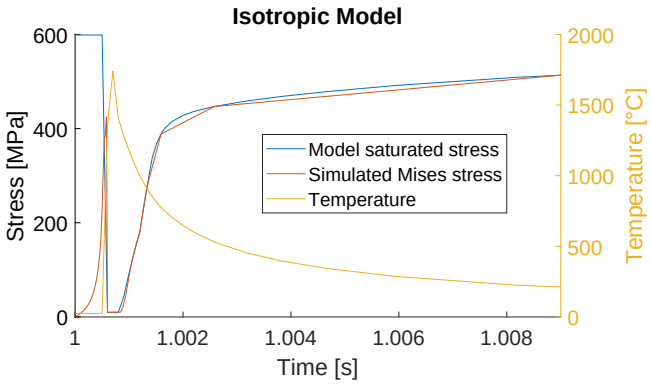

Figure 5.2: After a short transient phase, the simulated stress is governed by the model's saturated stress corresponding to the temperature field.

5.2. Isotropic and Kinematic Hardening

In Fig. 5.3, the simulated responses over time are plotted for both a kinematic and an isotropic simulation. Significant differences in responses between isotropic and kinematic hardening laws appear at lower layers, when more than two layers are printed on top. After four deposited layers, the residual stresses are 598.67 MPa with isotropic hardening and 584.31 MPa with kinematic hardening, which is 2.4% lower. After the complete five-layer simulation, the difference is larger, resulting in 598.78 Mpa with isotropic hardening and only 493.23 MPa with kinematic hardening, which is 18% lower. It is suspected that for larger simulations involving more than five layers, this difference would grow even further. The deviations may also be larger for hardening models that do not saturate as quickly, because the residual stress in the isotropic simulation is bounded by saturation. For the equivalent plastic strain (PEEQ), the choice of hardening model also has an influence. The final value in the simulation was 7.38% for isotropic and 7.58% for kinematic hardening, which is 3% higher.
Although the loading case is already cyclic for a layer when two subsequent layers are deposited on top, the applied stresses are in tension and release only. Annealing also has an influence, as hardening is reset at the top two layers. It can be seen in Fig 5.4 that the loading becomes fully cyclic once more than three layers have been deposited on top. This immediately leads to the observed differences in stress and strain levels.

5.3. Creep

Abaqus does not reset the equivalent creep strain (CEEQ) when the temperature rises beyond anneal temperature, yet it is not reasonable to accumulate creep strain for a molten material. The data in the plot was therefore reset when post-processing the data by subtracting accumulated creep strain before and during melting.
When simulating the deposition of a single track, the accumulated creep strain amounts to less than $2{\cdot}10^{-6}$ (Fig. 5.5, left), which is less than 0.1 % of the total plastic deformation

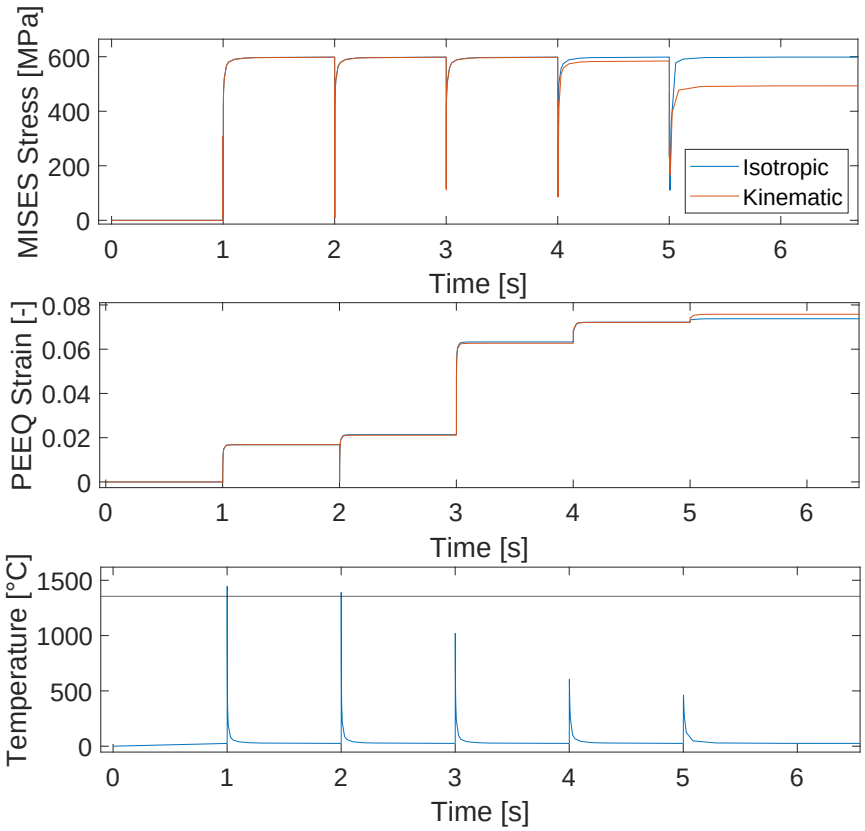

Figure 5.3: Simulated responses for isotropic and kinematic hardening model.

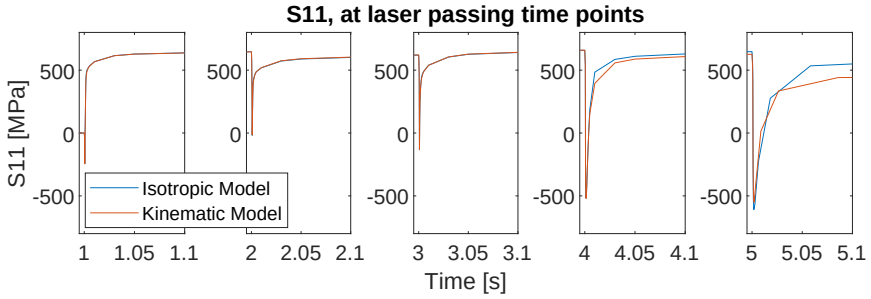

Figure 5.4: For lower layers, the loading becomes increasingly cyclic, resulting in a difference between isotropic and kinematic model response.

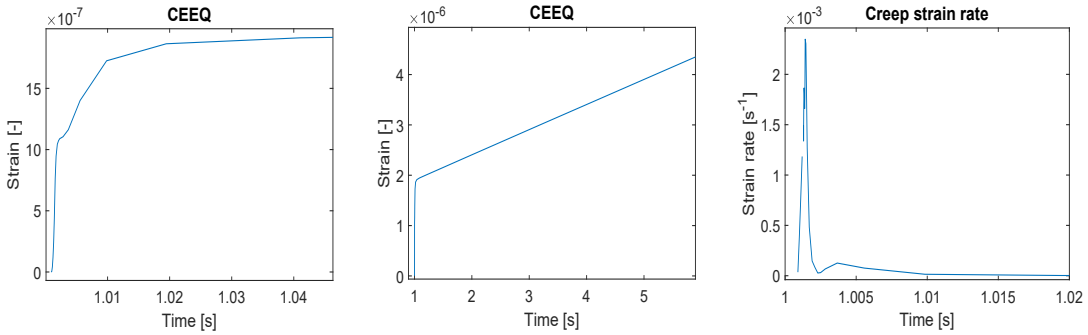

Figure 5.5: CEEQ during printing pulse(left), CEEQ during complete simulation time (middle), corresponding creep strain rate (right).

of such a simulation. The creep strain rate reaches relatively large values, but only for a very short time (Fig. 5.5, right). Even though stresses arrive at very high values, elevated temperatures at which significant creep straining could evolve are reached only for an extremely short amount of time. Furthermore, the amount of creep accumulated after cool-down is larger than the creep accumulated at high temperatures (Fig. 5.5, middle). For this small single track model, all material cools down below $100°C$ in the first 30 ms of cool-down. For larger, component scale prints, or in the case when the powder bed is preheated significantly, this far field temperature will be higher, which would result in a much larger amount of creep after cool-down.
The effect of creep on residual stress was extremely small, with only a difference of 0.24 MPa caused by stress relaxation, compared to 598.5 MPa of residual stress. This is partly because of the simple hardening law, which saturates rapidly (Section 5.1), but also because of the rather small total creep strain.
Including creep into an FEM simulation of LPBF took at least four times extra computational effort. The step time in creep simulations is limited by the maximum amount of creep strain per step. Because creep is extremely localized during the LPBF process, the excessive creep strain rate of a few elements slows down the entire simulation.

5.4. Annealing Effect

For the studied set, PEEQ ranges from 6.7 % to 7.4 %, showing a nearly linear dependence on anneal temperature, plotted in Fig. 5.6 on the right hand side. For all employed anneal temperatures, annealing is performed on each layer while it is deposited and also while the next layer is deposited (Fig. 5.6, left). The linear trend would drastically change, if annealing was performed more or less than two times on each layer. While the linear dependency is significant, it is of a greater importance to ensure that annealing is performed as often on each layer as intended. The differences on PEEQ can be accounted mostly to the linear shrinkage of the material with falling temperature. When the anneal temperature is set higher, a larger part of that cooling shrinkage is accumulated, leading

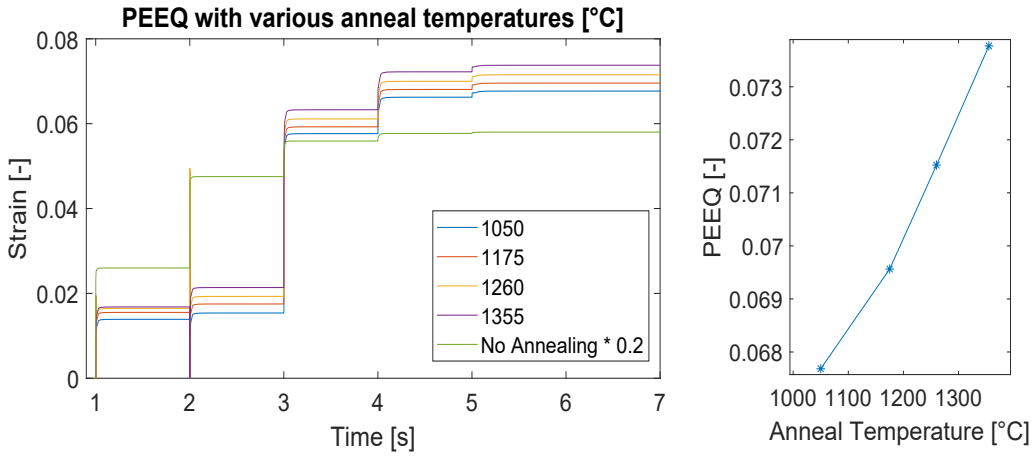

Figure 5.6: Influence of the anneal temperature on PEEQ: PEEQ over time (left), final PEEQ value depending on anneal temperature (right).

to a higher PEEQ. When no annealing is considered, the total PEEQ is about five times as large as most plastic straining occurs during the first two seconds, which would be annealed almost completely.

6. Conclusions

The sensitivity of residual stress and distortion development to the choice of constitutive model in simulations of LPBF additive manufacturing has been investigated. It was found that employing a kinematic hardening model has clearly an influence on the predicted residual stresses and distortions due to the reverse loading and cyclic nature of LPBF. It can be concluded that a lower simulation error can be expected when an appropriate constitutive model is fitted to cyclic test data.
In the case of creep, it was observed that the amount of creep directly induced by the laser in the vicinity of the localized heat input is negligible due to rapid cooling. But it is clear that elevated far-field temperatures caused by preheating or a larger print size could result in considerable stress relaxation, since the residual stresses are very large. When this is found to be the case, further research could be conducted about the implementation of creep behavior in a low-temperature domain, such that the simulation is not needlessly slowed down by the localized excessive creep strain rates.
It was shown that the material's annealing behavior must be treated in some way, otherwise non-usable excessive levels of PEEQ are recorded if it is omitted. Over a broad range, a nearly linear dependence of anneal temperature and PEEQ was found. While it would be hard to calibrate the anneal temperature using experiments, it is clear that a value close to melting temperature will be the most reasonable choice considering the rapid cool down, effectively limiting the time dependent diffusive processes behind annealing.
Finally, the hardening rules applied in this work suffered from fast saturation, which compromised the ability to see the effects the constitutive models had on stress. For further research, it would be beneficial to use experimental data reaching higher strain levels comparable to the occurring levels during the LPBF process, in order to rule out such limitations.

A. Appendix

	Anneal Temp [°C]	1355	Conductivity [W/mm.K]	Temp [°C]	Spec. Heat [J/kg.K]	Temp [°C]	Goldak Parameters	
	Expansion Coef. [-]	1.66E-05	1.03E-02	25	437.78	25	Subdiv x	20
	Density [kg/mm^3]	8.22E-06	1.16E-02	100	457.03	105	Subdiv y	20
Young's Mod [Mpa]	Poisson	Temp [°C]	1.34E-02	200	472.73	203	Subdiv z	20
183902.439	0.32	22	1.51E-02	300	488.83	305	a	0.05
173427.6144	0.32	200	1.69E-02	400	512.79	403	b	0.03
170320.568	0.23	400	1.89E-02	500	535.18	505	cf	0.05
156971.4989	0.32	600	2.08E-02	600	568.99	613	cr	0.05
145281.028	0.32	800	2.29E-02	700	597.72	624	ff	1
116614.1907	0.32	900	2.39E-02	800	603.59	698	fr	1
102909.8334	0.32	1000	2.60E-02	900	605.52	789	Box size	1
102909.8334	0.32	1355	2.81E-02	1000	609.83	834	AM Parameters	
			3.01E-02	1100	631.43	934	Laser Speed [mm/s]	1000
			3.23E-02	1200	647.15	998	Absorption Coef.	0.5
			3.46E-02	1260	667.97	1080	Film coefficient	1.00E-05
			5.53E-01	2060	684.86	1158	Sink temp	25
					709.20	1260	Emissivity	0.6
					709.20	1355		

Table A.1: Material Properties and AM modeller parameters.

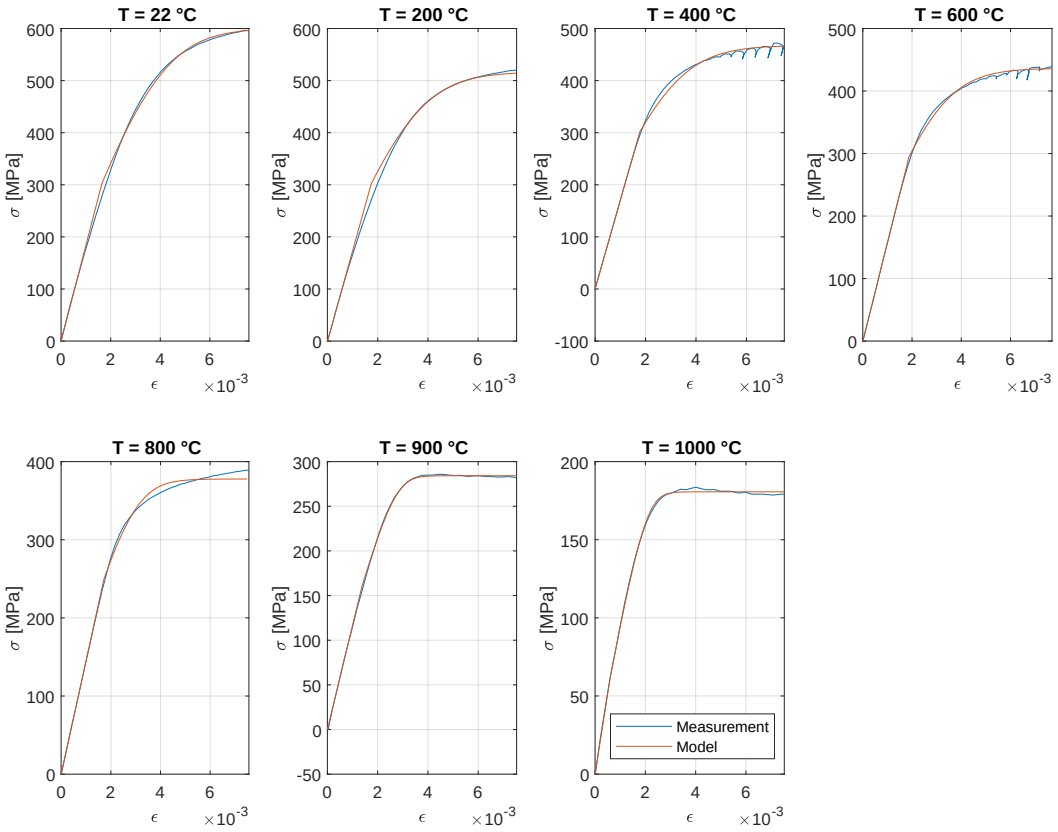

Figure A.1: First half cycle of tensile test: experimental data and elasto-plastic model

Nomenclature

List of Abbrevations

ϵ	[-]	Nominal strain in loading direction
ϵ_{pl}	[-]	Equivalent plastic strain
ϵ_{cr}	[-]	Nominal creep strain in loading direction
σ	[MPa]	Nominal stress
σ^0	[MPa]	Yield stress
σ_y	[MPa]	Yield stress at zero plastic strain
α	[MPa]	Backstress
E	[MPa]	Young's Modulus
Q_∞	[MPa]	Isotropic hardening parameter
b	[-]	Isotropic hardening parameter
C	[MPa]	Kinematic hardening parameter
γ	[-]	Kinematic hardening parameter
A	[MPa^{-n}]	Creep parameter
n	[-]	Creep paramter
t	[s]	Time

List of Figures

List of Tables

References

[1] Tarasankar DebRoy, HL Wei, JS Zuback, Tuhin Mukherjee, JW Elmer, JO Milewski, Allison Michelle Beese, A de Wilson-Heid, Amitava De, and W Zhang. Additive manufacturing of metallic components–process, structure and properties. *Progress in Materials Science*, 92:112–224, 2018.

[2] Amit Bandyopadhyay, Yanning Zhang, and Susmita Bose. Recent developments in metal additive manufacturing. *Current opinion in chemical engineering*, 28:96–104, 2020.

[3] Valeriya Griffiths, James P. Scanlan, Murat H. Eres, Antonio Martinez-Sykora, and Phani Chinchapatnam. Cost-driven build orientation and bin packing of parts in selective laser melting (slm). *European Journal of Operational Research*, 273:334–352, 2 2019. Image Source SLM schematic.

[4] Mika Salmi. Additive manufacturing processes in medical applications. *Materials*, 14(1):191, 2021.

[5] Andres Gasser, Gerhard Backes, Ingomar Kelbassa, Andreas Weisheit, and Konrad Wissenbach. Laser additive manufacturing laser metal deposition (lmd) and selective laser melting (slm) in turbo-engine applications. 2010.

[6] Martin Baumers, Phill Dickens, Chris Tuck, and Richard Hague. The cost of additive manufacturing: machine productivity, economies of scale and technology-push. *Technological forecasting and social change*, 102:193–201, 2016.

[7] Sheng Yang and Yaoyao Fiona Zhao. Additive manufacturing-enabled part count reduction: a lifecycle perspective. *Journal of mechanical design*, 140(3), 2018.

[8] Peter Mercelis and Jean-Pierre Kruth. Residual stresses in selective laser sintering and selective laser melting. *Rapid prototyping journal*, 2006.

[9] C. Li, Z. Y. Liu, X. Y. Fang, and Y. B. Guo. Residual stress in metal additive manufacturing. volume 71, pages 348–353. Elsevier B.V., 2018.

[10] Patcharapit Promoppatum and Anthony D. Rollett. Physics-based and phenomenological plasticity models for thermomechanical simulation in laser powder bed fusion additive manufacturing: A comprehensive numerical comparison. *Materials and Design*, 204, 6 2021.

[11] Laurent Van Belle, Guillaume Vansteenkiste, and Jean Claude Boyer. Comparisons of numerical modelling of the selective laser melting. volume 504-506, pages 1067–1072. Trans Tech Publications Ltd, 2012.

[12] S. Springer, A. Röcklinger, M. Leitner, F. Grün, T. Gruber, M. Lasnik, and B. Oberwinkler. Implementation of a viscoplastic substrate creep model in the thermomechanical simulation of the waam process. *Welding in the World*, 66:441–453, 3 2022.

[13] Robert Hurlston. Isotropic, kinematic or mixed-mode? which hardening model for your abaqus fea analysis?, 2021. `https://www.fidelisfea.com/post/isotropic-kinematic-or-mixed-mode-which-hardening-model-for\-your-abaqus-fea-analysis` [Accessed: 2022-05-16].

[14] Simulia. Abaqus documentation, 2021.

[15] Inc. Haynes International. Hastelloy x alloy manual. 1997.

[16] Harry Chandler. *Heat treater's guide: practices and procedures for nonferrous alloys*. ASM international, 1996.

[17] Xiaopeng Cheng, Zunfeng Du, Si Xu Chu, Jin Wu, Ji Dong, Hui Wang, and Zongqing Ma. The effect of subsequent heating treatment on the microstructure and mechanical properties of additive manufactured hastelloy x alloy. *Materials Characterization*, 186, 4 2022.

Eidgenössische Technische Hochschule Zürich
Swiss Federal Institute of Technology Zurich

Eigenständigkeitserklärung

Die unterzeichnete Eigenständigkeitserklärung ist Bestandteil jeder während des Studiums verfassten Semester-, Bachelor- und Master-Arbeit oder anderen Abschlussarbeit (auch der jeweils elektronischen Version).

Die Dozentinnen und Dozenten können auch für andere bei ihnen verfasste schriftliche Arbeiten eine Eigenständigkeitserklärung verlangen.

Ich bestätige, die vorliegende Arbeit selbständig und in eigenen Worten verfasst zu haben. Davon ausgenommen sind sprachliche und inhaltliche Korrekturvorschläge durch die Betreuer und Betreuerinnen der Arbeit.

Titel der Arbeit (in Druckschrift):

Numerical Analysis of Residual Stress and Distortion in Laser Powder Bed Fusion Process: A Sensitivity Analysis to the Choice of Constitutive Model

Verfasst von (in Druckschrift):
Bei Gruppenarbeiten sind die Namen aller Verfasserinnen und Verfasser erforderlich.

Name(n):	**Vorname(n):**
Schär	Timon

Ich bestätige mit meiner Unterschrift:
- Ich habe keine im Merkblatt „Zitier-Knigge" beschriebene Form des Plagiats begangen.
- Ich habe alle Methoden, Daten und Arbeitsabläufe wahrheitsgetreu dokumentiert.
- Ich habe keine Daten manipuliert.
- Ich habe alle Personen erwähnt, welche die Arbeit wesentlich unterstützt haben.

Ich nehme zur Kenntnis, dass die Arbeit mit elektronischen Hilfsmitteln auf Plagiate überprüft werden kann.

Ort, Datum	**Unterschrift(en)**
Dübendorf, 25.05.2022	

Bei Gruppenarbeiten sind die Namen aller Verfasserinnen und Verfasser erforderlich. Durch die Unterschriften bürgen sie gemeinsam für den gesamten Inhalt dieser schriftlichen Arbeit.